Experimental Mechanics
https://doi.org/10.1007/s11340-024-01112-7

RESEARCH PAPER

Size Effects in Strength and Strain Hardening Behavior of Single-Crystal 7075 Aluminum Alloy Micropillars

H. Li[1] · D. Zhao[1,2] · Y. Cui[1,2] · C. Dan[2] · S. Ma[2] · L. Wang[2] · J. Liu[2] · Y. Li[2] · Z. Chen[1,2] · H. Wang[1,2]

Received: 31 May 2024 / Accepted: 30 August 2024

Abstract

Background The size effect and deformation instability exhibited by materials at the micro- and nano-scale constrain the development and application of miniaturized devices. Introducing different defects in materials through different technical means to improve the deformation stability of materials has been the main research point of micro- and nano mechanics.

Objective This paper presents a novel strategy to completely eliminate the instability of microscopic deformations by the introduction of high-density precipitates in aluminum alloys by means of suitable heat treatment.

Methods A suitable heat treatment is used to introduce a high density of precipitates in the 7075 aluminum alloy. Using the Focused Ion Beam technique and in situ micropillar compression tests, micron-sized single-crystal micropillars were fabricated and the size dependence of the strength and strain-hardening behavior of 7075 aluminum alloy was systematically analyzed.

Results Compared with precipitate-free Al–Mg alloy micropillars, the micropillars fabricated from 7075 aluminum alloy exhibited more stable deformation behavior, predominantly due to the impediment of dislocation motion by precipitates. The power-law exponent for yield strength relative to pillar size was determined to approach a near-zero value, indicating a negligible dependency of yield strength on specimen size. Similarly, the smaller the size of micropillar, the higher the hardening rate, which can be rationalized by exhaustion hardening.

Conclusions The proposed method can eliminate the size effect of materials with pillar size above 0.5 μm and leads to a stabilization in deformation behavior. These are advantageous for the application of micro- and nano-sized components in advanced engineering systems.

Keywords Size effect · Aluminum alloy · Yield strength · Strain hardening behavior

Introduction

In contemporary technology, particularly for miniaturized devices, a comprehensive understanding of the mechanical behavior of materials at reduced specimen sizes is essential. Unlike bulk metallic materials, where deformation is predominantly controlled by forest dislocations, materials at nano- and micro-scales exhibit distinctive characteristics. These include size-dependent flow stress [1–5], plastic instability characterized by strain bursts [6–9], and stochastic deformation patterns [10, 11]. The development of small-scale mechanical testing techniques has significantly advanced our understanding of these unique deformation mechanisms, contributing to efforts to stabilize the inherently unstable deformation behaviors of micro- and nano-sized materials [12].

The size effect on strength is typically characterized by a power-law relationship between the strength and the specimen size, described by the equation:

$$\sigma \propto D^{-m} \tag{1}$$

where σ represents the yield strength or flow stress, D the specimen size, and m the power-law exponent [13]. Face-centered cubic (FCC) single-crystal metals exhibit a pronounced size dependence of strength, with m values ranging

✉ D. Zhao
zhaodechao95@sjtu.edu.cn

✉ Y. Cui
yccui@sjtu.edu.cn

[1] State Key Laboratory of Metal Matrix Composites, Shanghai Jiao Tong University, Shanghai 200240, PR China

[2] School of Materials Science and Engineering, Shanghai Jiao Tong University, Shanghai 200240, PR China

Published online: 18 September 2024

from 0.6 to 1, influenced by the stacking fault energy (SFE) of the material [1, 2, 4, 14, 15]. For instance, Al, with its relatively high SFE, exhibits an m value around 0.6, whereas Ag, with a lower SFE, shows an m value up to 0.9. Body-centered cubic (BCC) metals display lower m values, typically between 0.2 and 0.5, attributed to higher lattice friction stresses [16–18]. Several mechanisms have been proposed to explain the deformation behavior at reduced scales, including dislocation starvation [2], the weakest link [19], source truncation or single-arm source [20], and source exhaustion[21]. When the sample size falls below a characteristic material length scale [22], unique small-scale phenomenon gets activated like the material's plastic zone size or fracture process zone size [23, 24], since the role of free surfaces can not be neglected. Dislocations may escape from the material's surface, perpetuating a dislocation-starved condition necessitating higher stresses for the generation of new dislocations and subsequent plastic deformation. Furthermore, conventional double-ended Frank-Read dislocation sources may be truncated by the free surface, resulting in single-arm sources (SAS) that dominate further plastic deformation [25].

Although the "smaller is stronger" paradigm can substantially enhance material strength, potentially approaching theoretical values, the facile loss of dislocations and dislocation sources from the surfaces of single crystals can lead to jerky deformation behaviors and a reduction in plasticity. This is particularly problematic for micro-scale structural components. Various strategies, including the introduction of surface coatings [26], grain boundaries [27], and specific dislocation structures [28], have been explored to trap dislocations within the specimen, thereby improving strength and mitigating serrated flow. Experimental investigations have indicated that the presence of precipitates in alloys such as Al-Cu [29], Al-Cu-Mg [30], Mg-Zn [31], Ni-based alloy [32], and Ti alloy [33] directly influences the deformation behavior of micropillars, affecting size effects, strain hardening rates, and deformation stability. Ng et al. [34]found that compared to pure Al micropillars, the plastic instability and size effect are suppressed with the introduction of Guinier–Preston–Bagaryatsky (GPB) zones or S phase, and the suppression effect is related to precipitate diameter (d) and spacing (λ). Micropillars with nano-sized and spacing (GPB) zones exhibit smaller m values, but still exhibit certain plastic instability. Bellon et al.[29] obtained slightly different results when studying the effect of precipitate type on the deformation behavior of Al-Cu alloy micropillars. Micropillars containing nano-sized Guinier–Preston (GP) zones showed certain plastic instability due to precipitate shearing by dislocations. However, when the precipitates changed into submicron-sized θ phase (d ~ 400 nm), both plastic instability and size effect are well suppressed. Lavernia et al. [35] noted that precipitates could exacerbate plastic instability in submicron-aged 7075 Al pillars, highlighting the ongoing need to clarify the role of precipitates in influencing mechanical properties at micro-scales.

In this study, high-density second-phase nano-particles were introduced into an Al alloy through heat treatment. Selected grains, capable of activating a single slip system, were used to fabricate micropillars. Employing in situ micropillar compression testing, we analyzed the effects of these precipitates on both the deformation and strain hardening behaviors, elucidating the underlying mechanisms that govern these phenomena.

Material and Methods

Commercial extruded 7075 Al alloy was used in this study. The chemical composition, determined via inductively coupled plasma mass spectrometry (ICP-MS), was Al-5.2Zn-2.3 Mg-1.5Cu. For comparative study, as-extruded Al-6 Mg alloy was fabricated and held at 400 °C for 24 h. No precipitation phase will be formed inside Al-6 Mg alloy after heat treatment (natural aging will still occur after long-term solid solution of 7075 aluminum alloy), and compared with pure aluminum, its dislocation recovery after deformation will be hindered by solute atoms, which is conducive to a more realistic reflection of its hardening behavior. To achieve larger grains and eliminate dislocations, the specimens underwent solution treatment at 480 °C for 24 h in an air furnace, followed by peak aging at 120 °C for 24 h. Mechanical polishing, culminating in a final finish with a 0.04 μm silica sol suspension, was performed to minimize surface stress. The crystallographic orientation and grain size of the specimens were characterized using electron backscattered diffraction (EBSD) on a Tescan Lyra-3 scanning electron microscope (SEM) equipped with an Oxford EBSD detector, operating at an acceleration voltage of 20 kV and a step size of 4.8 μm. The EBSD data were analyzed with Aztec Crystal software. A grain with a [-5 4 12] orientation, favoring a single slip system, was selected for micropillar preparation. Considering that 7075 Al alloy at solid solution state will still undergo natural aging, while pure Al is prone to dislocation recovery during deformation, micropillars fabricated from Al6Mg alloys without precipitates were also examined for comparative purposes.

Cylindrical micropillars with diameters of about 0.5, 1, 3, and 5 μm and an aspect ratio of ~ 1:2 were fabricated at the center of the selected grain using a focused ion beam (FIB) in a Tescan Lyra-3 dual-beam SEM with Ga^+ ions operated at 30 kV. Final polishing was conducted using a 100 pA current to minimize surface damage and reduce the taper angle. All the micropillars had a taper angle of less than 2°. In situ micropillar compression tests were performed using an Alemnis standard assembly (ASA) nanoindentation

platform inside the SEM. A diamond cylindrical flat punch with a diameter of 10 μm was used to compress the pillars. All tests were conducted in displacement-controlled mode with a nominal strain rate of 0.001 s^{-1}. To ensure data consistency, at least five pillars of each size were tested, with representative curves presented in this manuscript. The engineering stress was calculated by dividing the load by the initial cross-sectional area at half-height, and the strain was corrected using a Sneddon correction to account for deformation of the substrate and indenter [36, 37].

$$x = x_{meas} - \frac{1-v_i^2}{E_i}\left(\frac{F_{meas}}{D_{top}}\right) - \frac{1-v_b^2}{E_b}\left(\frac{F_{meas}}{D_{bottom}}\right) \quad (2)$$

where x_{meas} is the displacement and F_{meas} is the load, D_{top} and D_{bottom} are the diameter at the top and bottom of the pillar, E_i and υ_i stand for the elastic modulus (1140 GPa) and Poisson' ratio (0.07) of diamond, while E_b and υ_b stand for the elastic modulus and Poisson' ratio of the 7075 alloy, respectively.

The engineering stress and engineering strain were converted into true stress and true strain by the following equation:

$$\sigma_t = \sigma_e\left(1+\varepsilon_e\right) \quad (3)$$

$$\varepsilon_t = \ln\left(1+\varepsilon_e\right) \quad (4)$$

where $\sigma_e, \sigma_t, \varepsilon_e, \varepsilon_t$ represent engineering stress, true stress, engineering strain, true strain, respectively. It should be noted that the engineering strain should be a negative value during the compression tests.

After deformation, thin foils parallel to the (110) slip plane of the single crystal were extracted from the micropillars using FIB. Transmission electron microscopy (TEM) and scanning TEM (STEM) observations were conducted using a Talos F200X G2 microscope at 200 kV to examine the distribution of precipitates and the dislocation structure. Dislocation types were identified under different two-beam conditions, where dislocations became invisible under extinction conditions.

Results

After heat treatment, the grain structure of the alloy along the extrusion direction exhibited a characteristic banded structure with bands approximately tens of micrometers in width, as illustrated by the EBSD orientation map in * MERGEFORMAT Fig. 1(a). The orientations along the observation direction are represented in the inverse pole figure (IPF), where a single slip system activation is indicated for the selected grain, as highlighted by the black dashed line. The primary slip system, identified through Schmid factor (SF) calculations, is $\left(11\bar{1}\right)[011]$ with an SF of 0.46. * MERGEFORMAT Fig. 1(b) to (d) present bright-field TEM images, and * MERGEFORMAT Fig. 1(e) displays the corresponding elemental maps of Fig. 1(d). Notably, GP zones or η' phases with diameters ranging from 3 to 4 nm were uniformly distributed within the grain. Additionally, coarse precipitates rich in Cr and Mg, exhibiting various shapes, were also observed. No dislocation lines were

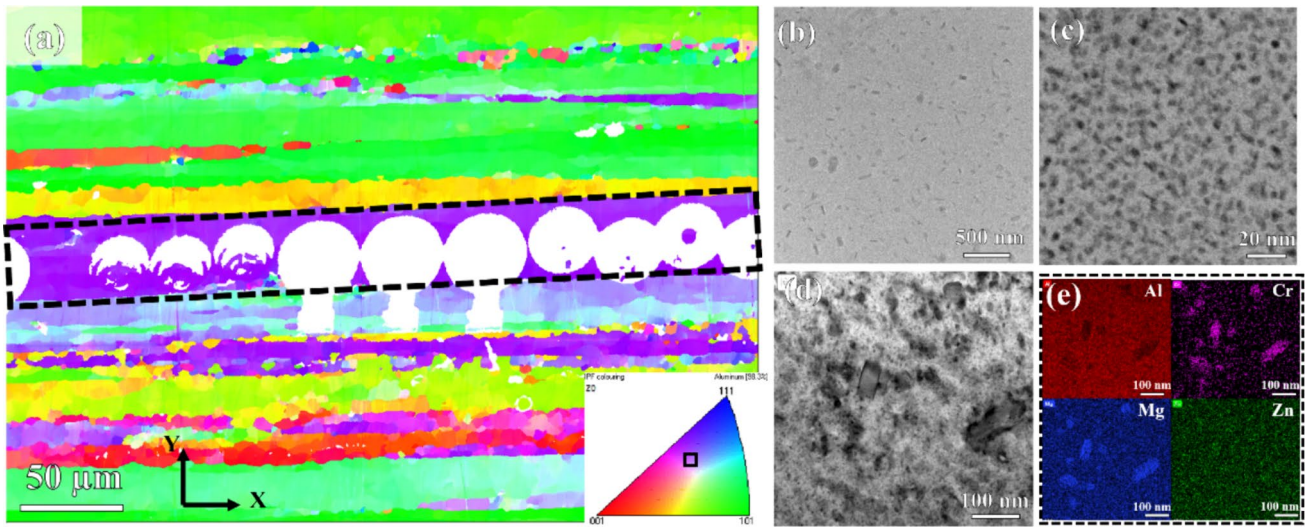

Fig. 1 Microstructure of the peak-aged 7075 alloy. (**a**) EBSD image showing the grain orientation and the grain selected. (**b**) bright-field TEM image of pillar prior to test; (**c**) and (**d**) TEM image showing a high density of second phase particles; (**e**) the corresponding STEM element maps of (d)

discernible, indicating that the sample was in a dislocation-free state after solution heat treatment.

Figure 2 presents the stress–strain curves for micropillars of Al–Mg and 7075 Al alloy. In comparison to pure Al single crystals, which demonstrate a 5% flow stress of approximately 50 MPa [38], Al–Mg micropillars exhibit a considerably higher flow stress of 300 MPa. Micropillars of 7075 Al alloy show a more substantial increase, with flow stresses reaching up to 600 MPa. As depicted in Fig. 2a, Al–Mg micropillars of all sizes exhibit jerky deformation behavior, with stress drops frequently exceeding 30 MPa. Notably, as the pillar size increases, the stress–strain curves become significantly smoother. Figure 2c reveals a similar trend for 7075 alloy micropillars; however, a distinct characteristic is observed when the micropillar size is increased to 5 μm. At this size, the jerky deformation features are completely eliminated, and the overall deformation behavior closely approximates that of bulk samples [39]. Figure 2(b) and (d) show the relationship between the 0.2% offset yield stress ($\sigma_{0.2}$) and 5% flow stress ($\sigma_{5\%}$) with pillar diameter (D) for Al–Mg and 7075 Al alloy, demonstrating an approximate power-law dependence. For the Al–Mg alloy, the exponent *m* for the 5% flow stress is determined to be 0.37. In contrast, for the 7075 alloy, the size effect exponents are markedly lower, recorded at 0.038 for yield stress and 0.017 for the 5% flow stress. These near-zero values suggest that the size effect on yield strength is essentially negligible in the 7075 Al alloy.

Further analysis was conducted on the strain hardening behavior of the 7075 Al micropillars, revealing a notable dependence on pillar size. The hardening rate (Θ) was calculated based on the true stress–strain response, under the assumption of homogeneous deformation and volume conservation [40]:

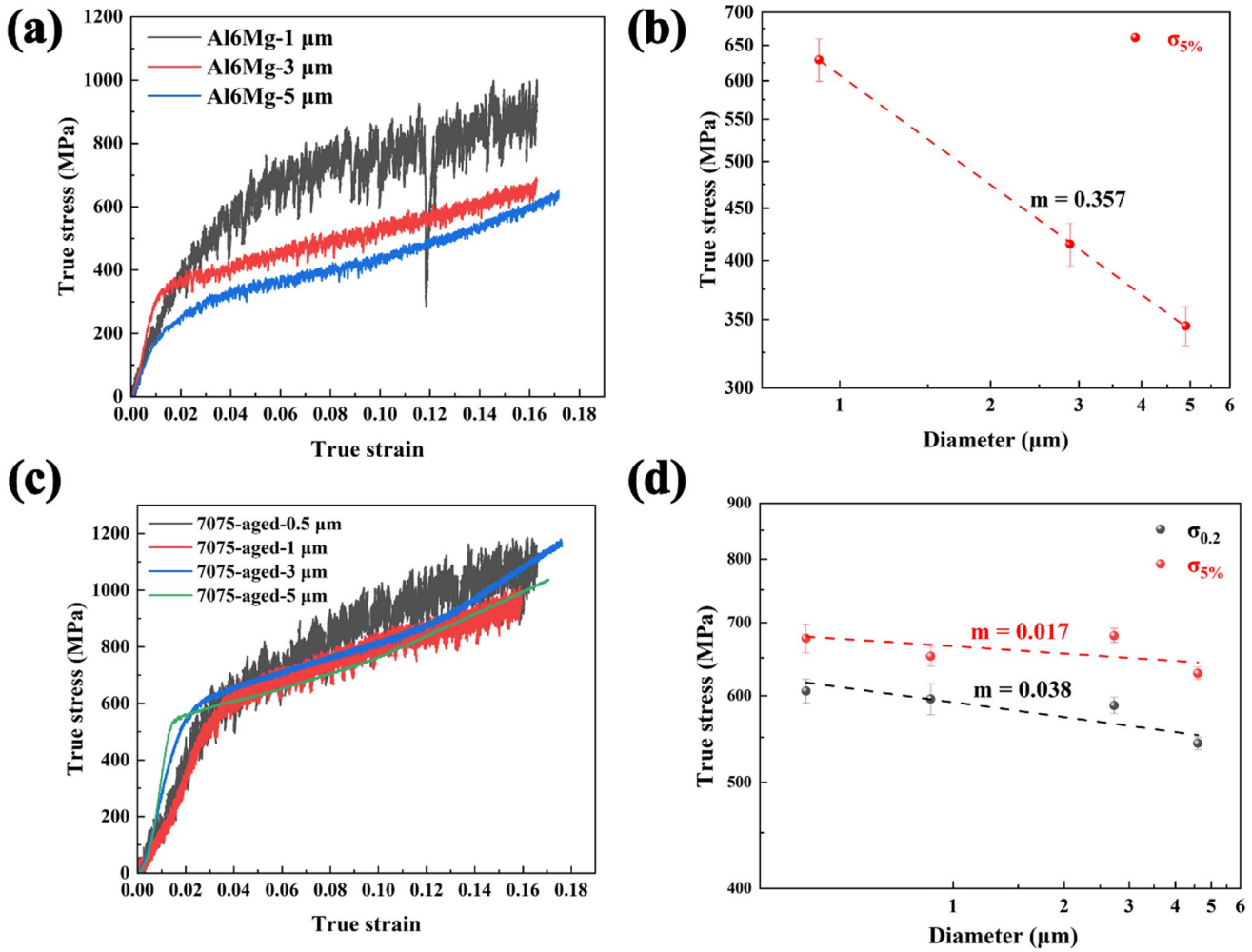

Fig. 2 (**a**) and (**c**) the stress-stain curves of AlMg with diameters of 1, 3 and 5 μm and 7075 micropillars with diameters of 0.5, 1, 3 and 5 μm. (**b**) 5% flow stress of AlMg micropillars versus pillar diameter. (**d**) the yield strength and flow stress at 5% compressive strain ($\sigma_{5\%}$) of micropillars versus pillar diameter

$$\Theta = \frac{\Delta\sigma_{true}}{\Delta\varepsilon_{true}} \tag{5}$$

This calculation was performed over a true strain range of 0.04 to 0.10, where a linear-plastic deformation was observable. The resulting values of Θ are illustrated in Fig. 3, showing a significant variance with D, similar to the aforementioned independence of yield stress on pillar size. The hardening rate peaked at 3.7 GPa for a pillar diameter of 0.5 μm, whereas it was lowest at 2.14 GPa for the 5 μm pillar.

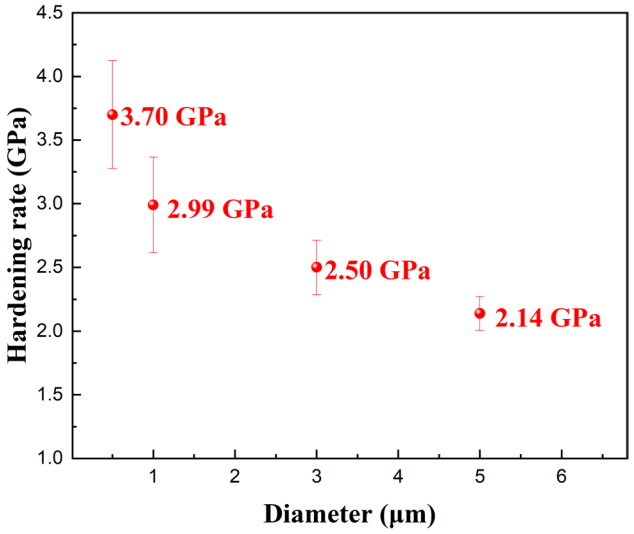

Fig. 3 Hardening rate determined from true stress–strain curves for micropillars of various size

An additional noteworthy observation is the presence of a distinct inflection point on the stress–strain curves for the 3 μm and 5 μm pillars in 7075 Al micropillars, indicative of an abrupt increase in the strain hardening rate—a phenomenon rarely reported in micropillar compression tests across various alloy systems [34, 41]. This increase in strain hardening accelerates the flow stress to 1 GPa for the 3 μm pillars and 1.3 GPa for the 5 μm pillars at 18% strain. Figure 4 presents typical scanning electron microscope (SEM) images of the pillars before and after deformation. For the 1 μm pillars, only parallel slip steps with a uniform distribution are observed across the pillar surfaces at both low and high strains (also see Supplementary Movie 1). Slip trace analysis demonstrates that these slip traces correspond to the primary slip system (1–11) [10-1], which exhibits the highest Schmid factor (SF) of 0.46. In contrast, the 5 μm pillars at 5% strain show more densely distributed slip steps, aligning with their smoother stress–strain response. As revealed by in situ SEM video analysis (Supplementary Movie 2), the appearance of a

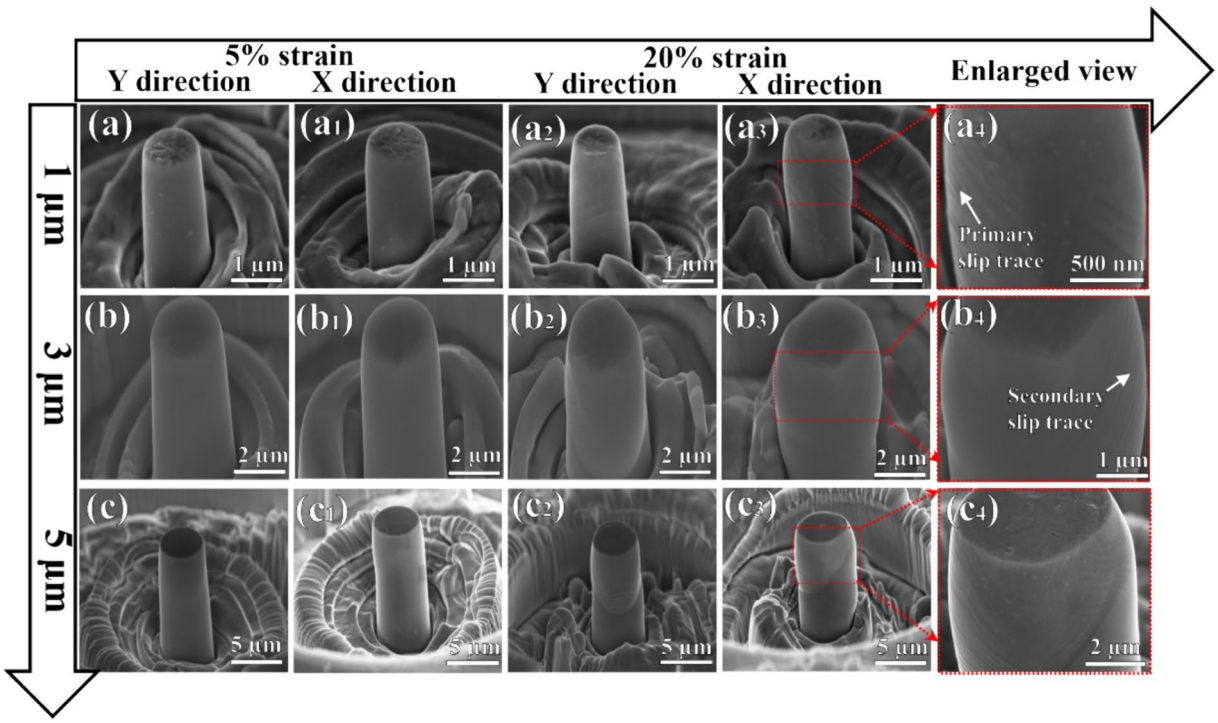

Fig. 4 SEM images of compressive 7075 micropillars of (**a**) 1 μm, (**b**) 3 μm and (**c**) 5 μm diameter. (a)-(a1), (b)-(b1), (c)-(c1) were taken along Y and X direction corresponding to the EBSD maps after 5% strain. (a2)-(a3), (b2)-(b3), (c2)-(c3) were taken along Y and X direction after 20% strain. (a4), (b4), (c4) are enlarged view of the area arrowed in (a3), (b3), (c3), respectively. All the images were taken at 45° titling angle

new set of slip steps intersecting the initial ones occurs around 10% strain. This development coincides with the inflection point on the stress–strain curves and signifies the activation of a secondary slip system.

Figure 5 presents bright-field TEM images of the 1 μm and 5 μm pillars after 5% strain. In the 1 μm pillar subjected to 5% strain, the dislocations were distributed homogeneously with a low density. Under the [11-1] two-beam condition, no dislocations were visible, indicating that most dislocations likely correspond to the same type, consistent with the single slip system favored by this pillar orientation. In contrast, the dislocations in the 5 μm pillar were distributed inhomogeneously. A region with a high density of dislocations (HDDS) was observed. During the TEM tilting process, the deformation zone (upper part in Fig. 5b) and the matrix (bottom part in Fig. 5b) reached the [110] zone axis successively. The tilt angles (α and β) exceeded 10°, indicating a misorientation angle of approximately 10° between these two regions. Compared to the dislocation starvation observed in pure Al micropillars [42], the dislocations were more effectively retained in both the 1 μm and 5 μm 7075 alloy pillars.

Discussion

The Effect of Precipitates on the Deformation Behavior

Plastic instabilities characterized by strain bursts and strain softening are significant issues for micro- and nano-sized specimens, adversely affecting the application of miniaturized components. Experimental results [43] and three-dimensional discrete dislocation dynamic simulations [9, 44] have demonstrated that strain bursts arise from the collective, avalanche-like motion of dislocations. A jammed configuration forms when dislocations become trapped by each other. When subsequent dislocations disrupt this jammed configuration, internal dislocations quickly annihilate through the pillar free surface in the form of dislocation avalanches, leading to large slip steps on the pillar surface. Another mechanism, the single-arm source mechanism, may also contribute to plastic instability [25]. A significant discrepancy exists between the dislocation nucleation rate generated by a single-arm source and the dislocation escaping rate. When single-arm sources leave the pillar surface,

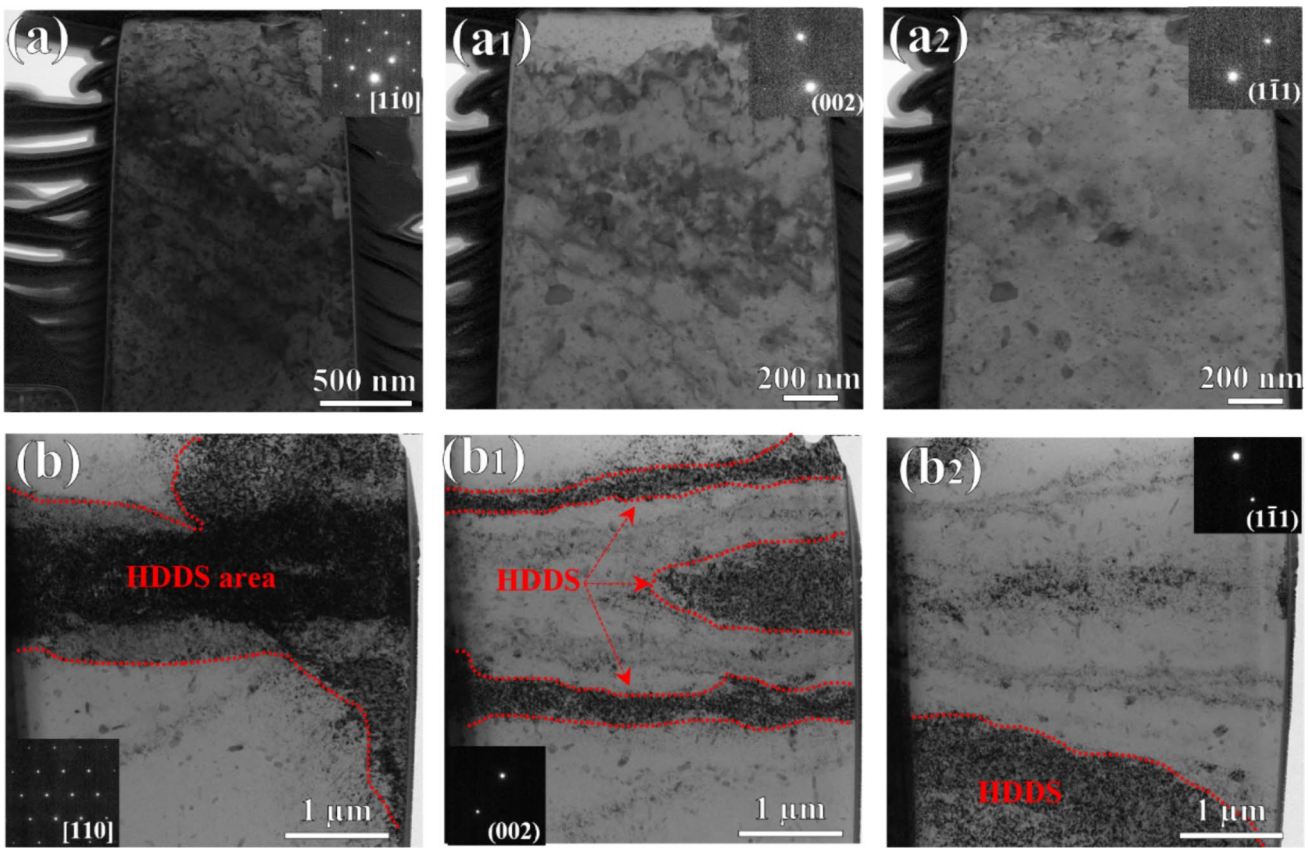

Fig. 5 TEM image showing the dislocation structures of (**a**) 1 μm and (**b**) 5 μm after 5% strain. (a) and (b) were taken under [110] zone axis, (a1) and (b1) were taken under g = [002] two-beam condition, and (a2) and (b2) were taken under g = [1–11] two-beam condition, respectively

the dislocation escaping rate exceeds the nucleation rate, causing strain bursts.

Compared to pure Al micropillars, the introduction of solute atoms (as in Al–Mg alloys, Fig. 2a-b) improves both the strength and deformation stability to some extent. However, even with larger micropillar sizes, deformation still exhibits jerky features, and strength shows a significant dependence on micropillar size. This suggests that solute atoms play a limited role and provide insufficient obstruction of dislocations and storage capacity. The introduction of dense precipitates in the 7075 alloy results in a near-zero size effect exponent while maintaining stable deformation with no strain bursts in stress–strain curves and faint slip steps on the pillar surface. The fine and dense η' precipitates act as strong barriers to dislocation motion, preventing dislocations from escaping the surface and leading to significant dislocation storage inside the pillars. As shown in TEM results (Fig. 5), a relatively high density of dislocations is observed in the 1 μm and 5 μm pillars after deformation. As pillar size decreases, mobile dislocations have a shorter path to the free surface with fewer encountered precipitates, explaining the consecutive stress drops in the 1 μm pillars. Lavernia [35] concluded that η' precipitates magnify the dislocation starvation mechanism, leading to more severe plastic instability in 7075 Al than in pure Al single crystals. The distinction between this work and our observation is likely due to the difference in pillar size. Compared to micro-sized pillars, the free surface of submicrometer pillars imposes a greater image force, attracting dislocations outward. Once precipitates fail to pin dislocations, more dislocations will be emitted from the surface.

Several works have reported that introducing different types of internal or external defects can alleviate the instability of deformation and the size effect of strength [26–28], but can never eliminate them. Our results demonstrate that the deformation behavior of single-crystal 7075 Al alloy micropillars is more stable than that of duralumin, which has precipitation of the S phase (Al_2CuMg) and GPB zones [34]. This results in relatively homogeneous deformation with minimal strain bursts and good strain hardening ability. Overall, the introduction of a high density of precipitates into micrometer-scale pillars is a good way to improve the deformation stability. When the size or spacing of the precipitates is small enough relative to pillar diameter (i.e., $D/d \approx 1000$ in present study), the deformation behavior can even be representative of bulk single crystals.

Origin of Non-Size Effect in 7075 Al Alloy

The dependence of σ_Y (τ_{CRSS}) on D is determined by the competition between the extrinsic length scale (i.e., the pillar diameter) and intrinsic microstructural length scale (i.e., grain size for polycrystal, dislocation cell size for pre-strained specimen, and precipitate size and spacing for heat-treated alloys) [23]. It is generally recognized only when the external length scale is 6 times greater than the internal length scale, the size effect can be effectively suppressed [45–47]. Variations in σ with D of pure Al, bi-crystal Al, pre-strained Al, cold-rolled Al and precipitation strengthened Al and the calculated m value are summarized in * MERGEFORMAT Fig. 6.

Pure Al holds the highest size effect exponent of about 0.85. In previous works, with the introduction of defects such as coatings, alloy elements and initial dislocations, the m value of Al alloys can be decreased from 0.8 to about 0.06. Our effect of introducing dense nano-precipitates further reduces the number to 0.003, suggesting that the Al pillars can have a size-independent deformation. For micro-scaled single crystals, single-arm dislocation sources (SASs) proposed by Parthasarathy [25] can describe the size dependence of strength, in which the critical resolved shear stress τ_{CRSS} to initiate macroscopic plastic deformation from a truncated weakest SASs with a statistical average length $\overline{\lambda}_{max}$ is described with the following equation:

$$\tau_{CRSS} = \tau_0 + \tau_p + \tau_D + \tau_S = \tau_{bulk} + \tau_S \approx \tau_0 + \tau_p + 0.5K_s b\sqrt{\rho} + \frac{\alpha K_s b}{\overline{\lambda}_{max}} \quad (6)$$

where τ_0, τ_p, τ_D and τ_S are the friction stress, stress contributed by precipitation strengthening, elastic interaction stress generally approximated as the Taylor hardening stress, and the source activation stress, respectively. K_s is the anisotropic shear modulus, b is the magnitude of Burgers vector, ρ is the total dislocation density, α is a geometrical constant. In previous studies, the sum of the first terms, $\tau_0 + \tau_p + \tau_D$ is normally assumed to be pillar size independent (bulk strength).

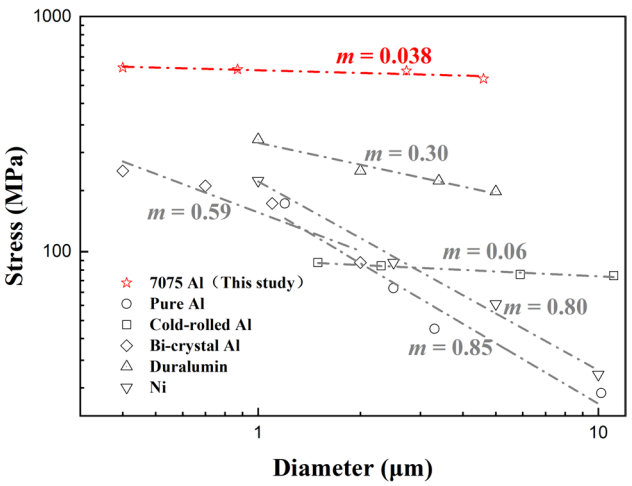

Fig. 6 The yield strength $\sigma_{0.2}$ as a function of pillar diameter in 7075 Al (this study), pure Al [28], Cold-rolled Al [28], Bi-Crystal Al [3], Duralumin [34], and pure Ni [14], respectively

Combined with Eq. (1) and (6), It can be inferred that the m value is determined by τ_{bulk} and τ_S, and we first consider the impact of precipitates on τ_{bulk} and m. The bulk CRSS value of pure Al single-crystal was conventionally used as 1 MPa [48], τ_{CRSS} was approximately 28 MPa for a D value of 1.4 μm and decreased with increasing D until saturation to 5 MPa at a critical diameter of 10 μm, much higher than the bulk strength [28]. Therefore, for pure Al single crystal pillars, size dependent τ_S dominates the pillars strength, resulting in a large size effect exponent. Combing Eq. (1) and Eq. (6), the m value of pure Al is about 0.72, which is in good agreement with the experimental results (0.6 ~ 0.9). With the introducing of dense precipitates, the yield strength of 7075 Al alloy increases significantly to 500 MPa. Considering that the alloy in this study has been sufficiently solution heat treated and all the micropillars were all fabricated in a single grain, solid solution strengthening and precipitate strengthening are supposed to be the major contributors of the yield strength, with grain boundary strengthening and dislocation strengthening being negligible. The predominant strengthening mechanism in peak-aged 7075 alloy has been determined to be precipitation Orowan strengthening, which contributes a strength increment of 414 MPa while the contribution from solid solution is below 82 MPa [39]. Summarizing the contributions of different strengthening mechanisms, the upper limit of the single crystal micropillar strength is supposed to be 525 MPa, close to the measured strength of the micropillars in this study. Taking the Schmid factor of pillar orientation into account, the theoretical value of m is calculated at 0.05. Good consistence between theoretical calculation and experiment demonstrates that the increase of the bulk strength caused by the introduction of dislocations or precipitates dominates the change of the size effect exponent.

Secondly, precipitates will have an effect on τ_S. From Eq. (6), τ_S is inversely proportional to the statistical average length $\overline{\lambda}_{max}$, and $\overline{\lambda}_{max}$ is a function of pillar size R and the number of pinning points n. The effective $\overline{\lambda}_{max}$ can be derived from the probability ($p(\lambda_{max})$) of having a pin with a single-arm dislocation source in a cylindrical micropillar with a certain radius (R) as follows:

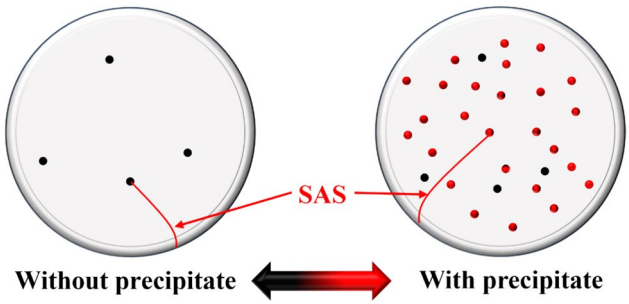

Fig. 7 Schematic illustration of the increment of $\overline{\lambda}_{max}$ because of the introducing of dense precipitates

$$\rho_{mobile} = \frac{\rho_{tot}}{s} \tag{9}$$

where λ_{max} is the effective source length, R is radius of cylindrical specimen, h is the micropillar height, L_{seg} is the average length of the single arm dislocation source, ρ_{tot} and ρ_{mob} are the total dislocation density and mobile dislocation density, respectively. The solute atoms and precipitates will serve as additional pinning points for SAS, resulting in a larger amount of pinning points (n) than that in pure Al, as illustrated in Fig. 7. The increment of n leads to an increase in $\overline{\lambda}_{max}$ and decrease in τ_S, which means that the stress contributed by single-arm dislocations in 7075 cannot be higher than that in pure Al. Therefore, the upper value 28 MPa was taken as the strength of single arm dislocation source. As a result, the size-effect exponent m should be smaller than 0.05 and the measured value (7075 Al) is only 0.038. The above two factors cause the size-independent behavior of strength of the 7075 alloy.

In fact, it has been reported [23] that when the internal scale parameter is one order of magnitude smaller than the micropillar size, the size effect on strength will be suppressed. In this paper, the size of the precipitated phase is nanometer-scale, and its spacing is only about 5 nm. In the range of micropillar sizes selected in this paper, d/D = 0.001 ~ 0.01, that is, the internal size parameter (d) is two to three orders of magnitude smaller than the external

$$\overline{\lambda}_{max} = \int_0^R \lambda_{max} p(\lambda_{max}) d\lambda_{max} = \int_0^R \left[1 - \frac{\pi(R-\lambda_{max})(b-\lambda_{max})}{\pi Rb}\right]^{n-1} \times \left(\frac{\pi\left[(R-\lambda_{max})+(b-\lambda_{max})\right]}{\pi Rb}\right) n\lambda_{max} d\lambda_{max} \tag{7}$$

$$p(\lambda_{max})d\lambda_{max} = \left[1 - \frac{\pi(R-\lambda_{max})(b-\lambda_{max})}{\pi Rb}\right]^{n-1} \left(\frac{\pi\left[(R-\lambda_{max})+(b-\lambda_{max})\right]}{\pi Rb}\right) n d\lambda_{max}$$
$$n = Integer\left[\rho_{mob}\frac{\pi R^2 h}{L_{seg}}\right] \tag{8}$$

size parameter (D). Therefore, it is reasonable that the size effect is completely suppressed, that is, the strength of the micropillar is completely controlled by the precipitates and is basically not affected by the size of the micropillars.

Strain Hardening Behavior of 7075 Al Alloy

Our experimental results show that the hardening rate of 7075 Al micropillars increases with decreasing size. The 0.5 μm micropillars exhibit the highest hardening rate (3.37GPa); while the 5 μm micropillars exhibit the lowest hardening rate (2.14 GPa). Similarly, Kiener et al. [40] have demonstrated through both experimental and simulation studies that smaller pillar sizes correspond to higher hardening rates, attributable to the increased density of geometrically necessary dislocations (GNDs) within smaller pillars.

Yield stress or critical resolved shear stress is associated with the generation of the first mobile dislocation or the activation of the primary slip system, and is thus directly linked to the activation of dislocation sources. Strain hardening behavior, on the other hand, is primarily governed by the capacity for dislocation storage, which in turn relates to the balance between dislocation multiplication and annihilation.

Based on present results and previous studies, two mechanisms are considered to be the possible origin of the size effects on hardening behavior—the progressively harder operation of dislocation sources with decreasing size, and the loss of dislocation sources in small volumes due to the more pronounced influence of surfaces [2], especially in the submicrometer regime (dislocation starvation/exhaustion) [20, 49]. Firstly, the smaller the size of the micropillar, the fewer the number of dislocation sources inside. As the deformation progresses, the dislocation sources will be constantly consumed, higher stresses are required to activate new dislocation sources. Secondly, as the size of the micropillar decreases, the role of the free surface becomes more and more prominent. The mobile dislocations within the micropillar only need to move a shorter distance to reach the free surface and then annihilate, making it increasingly difficult for dislocations to be stored within the micro-pillar through dislocation interactions. This is confirmed by the larger stress drop in the stress–strain curve (Fig. 2) and the lower dislocation density (Fig. 5) of the smaller micro-pillar. Once the mobile dislocations are annihilated through the free surface, higher stresses are required to generate new mobile dislocations. Dislocation starvation and the source exhaustion mechanism lead to the size dependence of the micropillar work hardening behavior. Indeed, factors such as crystal orientation, precipitate characteristics, and micropillar fabrication techniques also influence hardening behavior, suggesting that a more systematic investigation is required to fully understand strain hardening behavior at the micro-scale.

Conclusion

In this study, uniaxial compression tests were performed on single slip-oriented micropillars of Al–Mg and 7075 Al alloy. Analyzing the in situ test results and TEM dislocation characterizations, we investigated the size effects on deformation behavior, strength, and strain hardening ability. Our findings can be summarized as follows:

1. The introduction of solute atoms effectively suppresses the size effect and enhances deformation stability, although complete elimination of the size effect remains challenging.
2. With the incorporation of dense nano-precipitates, single crystal micropillars ranging from 0.5 μm to 5 μm in diameter exhibited enhanced plasticity and superior strain hardening capabilities. Remarkably, the size effect was virtually absent, with a size effect exponent of 0.017.
3. The independence of yield strength from pillar size in 7075 Al micropillars can be attributed to two main factors: (i) the strengthening effect of precipitates, which mitigates the influence of single-arm dislocation sources on overall strength, and (ii) the dense precipitates that provide additional pinning points for dislocation sources, thus increasing the average length of single-arm sources.
4. The size dependence of strain hardening ability is explained mainly by exhaustion hardening. The smaller the size of the micropillar, the fewer the number of dislocation sources, and the easier it is for the mobile dislocations to be annihilated through the free surface. Higher stress is required to generate new mobile dislocations to sustain plastic deformation.

The presence of finer and denser precipitates not only eliminates the commonly observed size effect of strength in microscale deformation but also provides a robust strain hardening capability. These attributes are advantageous for the application of micro- and nano-sized components in advanced engineering systems.

Acknowledgements Financial support of this work was obtained from National Natural Science Foundation of China, Grant Number 52201130 and 51971137, and Shanghai Science and Technology Committee Rising-Star Program, Grant Number 22YF1419300.

Author Contribution Hengfu Li: Methodology, Validation, Formal analysis, Investigation, Writing – original draft. Dechao Zhao: Conceptualization, Writing – review & editing. Yuchi Cui: Methodology, Supervision, Funding acquisition, Conceptualization, Formal analysis,

Writing – review & editing. Chengyi Dan: Formal analysis, Conceptualization. Siming Ma: Formal analysis, Writing – review & editing. Lei Wang: Formal analysis, Writing – review & editing. Jun Liu: Formal analysis, Writing – review & editing. Yang Li: Resources, Writing – review & editing. Zhe Chen: Supervision, Funding acquisition, Project administration, Conceptualization, Writing – review & editing. Haowei Wang: Supervision, Conceptualization.

Funding National Natural Science Foundation of China,52201130,Z. Chen,51971137,Z. Chen,Shanghai Science and Technology Committee Rising-Star Program,22YF1419300,Yuchi Cui

Data Availability Data will be made available on request.

Declarations

Competing Interest The authors declare that they have no known competing financial interests or personal relationships that could have appeared to influence the work reported in this paper.

References

1. Volkert CA, Lilleodden ET (2006) Size effects in the deformation of sub-micron Au columns. Philos Mag 86:5567–5579
2. Greer JR, Nix WD (2006) Nanoscale gold pillars strengthened through dislocation starvation. Phys Rev B 73:245410
3. Kunz A, Pathak S, Greer JR (2011) Size effects in Al nanopillars: Single crystalline vs. bicrystalline. Acta Mater 59:4416–4424
4. Wang Z-J, Li Q-J, Shan Z-W, Li J, Sun J, Ma E (2012) Sample size effects on the large strain bursts in submicron aluminum pillars. Appl Phys Lett 100(7):071906
5. Ng KS, Ngan AHW (2009) Effects of trapping dislocations within small crystals on their deformation behavior. Acta Mater 57:4902–4910
6. Greer JR, Oliver WC, Nix WD (2005) Size dependence of mechanical properties of gold at the micron scale in the absence of strain gradients. Acta Mater 53:1821–1830
7. Crosby T, Po G, Erel C, Ghoniem N (2015) The origin of strain avalanches in sub-micron plasticity of fcc metals. Acta Mater 89:123–132
8. Ryu I, Nix WD, Cai W (2013) Plasticity of bcc micropillars controlled by competition between dislocation multiplication and depletion. Acta Mater 61:3233–3241
9. Csikor FF, Motz C, Weygand D, Zaiser M, Zapperi S (2007) Dislocation Avalanches, Strain Bursts, and the Problem of Plastic Forming at the Micrometer Scale. Science 318:251–254
10. Ng KS, Ngan AHW (2008) Stochastic theory for jerky deformation in small crystal volumes with pre-existing dislocations. Philos Mag 88:677–688
11. Shao S, Abdolrahim N, Bahr DF, Lin G, Zbib HM (2014) Stochastic effects in plasticity in small volumes. Int J Plast 52:117–132
12. Wang Z, Shan Z, Li J, Sun J, Ma E (2014) An index for deformation controllability of small-volume materials. Sci China Technol Sci 57:663–670
13. Kraft O, Gruber PA, Mönig R, Weygand D (2010) Plasticity in Confined Dimensions. Annu Rev Mater Res 40:293–317
14. Dimiduk DM, Uchic MD, Parthasarathy TA (2005) Size-affected single-slip behavior of pure nickel microcrystals. Acta Mater 53:4065–4077
15. Wu JH, Tsai WY, Huang JC, Hsieh CH, Huang G-R (2016) Sample size and orientation effects of single crystal aluminum. Mater Sci Eng A 662:296–302
16. Heller M, Gibson JSKL, Pei R, Korte-Kerzel S (2020) Deformation of μm- and mm-sized Fe2.4wt%Si single- and bi-crystals with a high angle grain boundary at room temperature. Acta Mater 194:452–463
17. Yilmaz H, Williams CJ, Risan J, Derby B (2019) The size dependent strength of Fe, Nb and V micropillars at room and low temperature. Materialia 7:100424
18. Zhang J, Kishida K, Inui H (2017) Specimen size and shape dependent yield strength in micropillar compression deformation of Mo single crystals. Int J Plast 92:45–56
19. El-Awady JA, Wen M, Ghoniem NM (2009) The role of the weakest-link mechanism in controlling the plasticity of micropillars. J Mech Phys Solids 57:32–50
20. Kiener D, Minor AM (2011) Source truncation and exhaustion: insights from quantitative in situ TEM tensile testing. Nano Lett 11:3816–3820
21. Zhou C, Beyerlein IJ, LeSar R (2011) Plastic deformation mechanisms of fcc single crystals at small scales. Acta Mater 59:7673–7682
22. Zhao XX, Wu J, Chiu YL, Jones IP, Gu R, Ngan AHW (2019) Critical dimension for the dislocation structure in deformed copper micropillars. Scr Mater 163:137–141
23. Greer JR, De Hosson JTM (2011) Plasticity in small-sized metallic systems: Intrinsic versus extrinsic size effect. Prog Mater Sci 56:654–724
24. Patel ZS, Alrashed AO, Dwivedi K, Salviato M, Meza LR (2024) Rethinking ductility—A study into the size-affected fracture of additively manufactured polymers. Addit Manuf 84:104113
25. Parthasarathy TA, Rao SI, Dimiduk DM, Uchic MD, Trinkle DR (2007) Contribution to size effect of yield strength from the stochastics of dislocation source lengths in finite samples. Scr Mater 56:313–316
26. El-Awady JA, Rao SI, Woodward C, Dimiduk DM, Uchic MD (2011) Trapping and escape of dislocations in micro-crystals with external and internal barriers. Int J Plast 27:372–387
27. Imrich PJ, Kirchlechner C, Motz C, Dehm G (2014) Differences in deformation behavior of bicrystalline Cu micropillars containing a twin boundary or a large-angle grain boundary. Acta Mater 73:240–250
28. Takata N, Takeyasu S, Li H, Suzuki A, Kobashi M (2020) Anomalous size-dependent strength in micropillar compression deformation of commercial-purity aluminum single-crystals. Mater Sci Eng A 772:138710
29. Bellón B, Haouala S, Llorca J (2020) An analysis of the influence of the precipitate type on the mechanical behavior of Al - Cu alloys by means of micropillar compression tests. Acta Mater 194:207–223
30. Gu R, Leung PPS, Ngan AHW (2014) Size effect on deformation of duralumin micropillars – A dislocation dynamics study. Scr Mater 76:73–76
31. Wang CY, Cepeda-Jiménez CM, Pérez-Prado MT (2020) Dislocation-particle interactions in magnesium alloys. Acta Mater 194:190–206
32. Cruzado A, Gan B, Jiménez M, Barba D, Ostolaza K, Linaza A, Molina-Aldareguia JM, Llorca J, Segurado J (2015) Multiscale modeling of the mechanical behavior of IN718 superalloy based on micropillar compression and computational homogenization. Acta Mater 98:242–253
33. Chen W, Zhang J, Cao S, Pan Y, Huang M, Hu Q, Sun Q, Xiao L, Sun J (2016) Strong deformation anisotropies of ω-precipitates and strengthening mechanisms in Ti-10V-2Fe-3Al alloy micropillars: Precipitates shearing vs precipitates disordering. Acta Mater 117:68–80
34. Gu R, Ngan AHW (2013) Size effect on the deformation behavior of duralumin micropillars. Scr Mater 68:861–864

35. Hu T, Jiang L, Yang H, Ma K, Topping TD, Yee J, Li M, Mukherjee AK, Schoenung JM, Lavernia EJ (2015) Stabilized plasticity in ultrahigh strength, submicron Al crystals. Acta Mater 94:46–58
36. Ding J, Li Q, Li J, Xue S, Fan Z, Wang H, Zhang X (2018) Mechanical behavior of structurally gradient nickel alloy. Acta Mater 149:57–67
37. Frick CP, Clark BG, Orso S, Schneider AS, Arzt E (2008) Size effect on strength and strain hardening of small-scale [111] nickel compression pillars. Mater Sci Eng A 489:319–329
38. Ng KS, Ngan AHW (2009) Deformation of micron-sized aluminium bi-crystal pillars. Philos Mag 89:3013–3026
39. Ma K, Wen H, Hu T, Topping TD, Isheim D, Seidman DN, Lavernia EJ, Schoenung JM (2014) Mechanical behavior and strengthening mechanisms in ultrafine grain precipitation-strengthened aluminum alloy. Acta Mater 62:141–155
40. Kiener D, Guruprasad PJ, Keralavarma SM, Dehm G, Benzerga AA (2011) Work hardening in micropillar compression: In situ experiments and modeling. Acta Mater 59:3825–3840
41. Gu R, Ngan AHW (2013) Dislocation arrangement in small crystal volumes determines power-law size dependence of yield strength. J Mech Phys Solids 61:1531–1542
42. Ng KS, Ngan AHW (2008) Stochastic nature of plasticity of aluminum micro-pillars. Acta Mater 56:1712–1720
43. Oh SH, Legros M, Kiener D, Dehm G (2009) In situ observation of dislocation nucleation and escape in a submicrometre aluminium single crystal. Nat Mater 8:95–100
44. Senger J, Weygand D, Gumbsch P, Kraft O (2008) Discrete dislocation simulations of the plasticity of micro-pillars under uniaxial loading. Scr Mater 58:587–590
45. Dehm G, Jaya BN, Raghavan R, Kirchlechner C (2018) Overview on micro- and nanomechanical testing: New insights in interface plasticity and fracture at small length scales. Acta Mater 142:248–282
46. Kiener D, Hosemann P, Maloy SA, Minor AM (2011) In situ nanocompression testing of irradiated copper. Nat Mater 10:608–613
47. Girault B, Schneider AS, Frick CP, Arzt E (2010) Strength Effects in Micropillars of a Dispersion Strengthened Superalloy. Adv Eng Mater 12:385–388
48. Hosford Jr WF, Fleischer RL, Backofen WA (1960) Tensile deformation of aluminum single crystals at low temperatures. Acta Metall 8(3):187–199
49. Nix WD, Lee S-W (2011) Micro-pillar plasticity controlled by dislocation nucleation at surfaces. Philos Mag 91:1084–1096